Evidences for pressure-induced two-phase superconductivity and mixed structures of $NiTe_2$ and NiTe in type-II Dirac semimetal $NiTe_{2-x}$ ($x = 0.38 \pm 0.09$) single crystals

Zhenjie Feng[1*], Jingying Si[1], Tao Li[1], Hongliang Dong[2], Chunqiang Xu[3], Jiong Yang[1], Zhou Zhang[1], Ke Wang[1, 2], Hao Wu[1, 2], Qiang Hou[1], JuanJuan Xing[1], Shun Wan[2], Shujia Li[2], Wen Deng[2], Jiajia Feng[2], Arnab Pal[1], Fei Chen[1], Shunbo Hu[1], Jun-Yi Ge[1], Cheng Dong[4], Shenghao Wang[1], Wei Ren[5], Shixun Cao[1, 5], Yi Liu[6], Xiaofeng Xu[6], Jincang Zhang[1*], Bin Chen[2*], Nai-Chang Yeh[7*]

[1]*Materials Genome Institute, Shanghai University, Shanghai, 200444, China*

[2]*Center for High Pressure Science and Technology Advanced Research, Shanghai 201203, China*

[3]*School of Physics and Key Laboratory of MEMS of the Ministry of Education, Southeast University, Nanjing 211189, China*

[4]*School of Advanced Materials, Peking University Shenzhen Graduate School, Shenzhen 518055, Guangdong, China*

[5]*Shanghai Key Laboratory of High Temperature Superconductors, Department of Physics, Shanghai University, Shanghai, 200444, China*

[6] *Department of Applied Physics, Zhejiang University of Technology, Hangzhou, 310023, China*

[7]*Department of Physics, California Institute of Technology, Pasadena, CA 91125, USA*

Supporting Information:

Materials and Methods

Figures S1-S10

The supplementary information consists of texts and related figures (Figures S1-S10) that describe methods in the following five sections: 1) XRD powder spectrum of $NiTe_{2-x}$ under ambient pressure; 2) Electron diffraction spectroscopy (EDS) analyses of the $NiTe_{2-x}$ compositions; 3) Results from the density functional theory (DFT) calculations: [1] Electronic density of states (DOS) of NiTe (M-phase) under high pressures P = 18 and 42 GPa, and of $NiTe_2$ and $NiTe_{1.625}$ (H-phase) at P = 0 (Figures. S6a-d); [2] Comparison of the DOS of $NiTe_2$ (H-phase) under P = 0, 18 and 42 GPa (Figures. S7a-c); [3] First Brillouin zones of $NiTe_2$ (H-phase, Figure. S8a) and NiTe (M-phase, Figure. S8b); [4] Comparison of the electronic bandstructures of $NiTe_2$ (H-phase, P = 0, Figure. S9a) and NiTe (M-phase, P = 18 GPa, Figure. S9b); [5] Comparison of the electronic bandstructures of $NiTe_2$ (H-phase, P = 18 GPa, Figure. S10a) and $NiTe_2$ (H-phase, P = 42 GPa, Figure. S10b).

Materials and Methods:

1. XRD powder diffraction pattern of $NiTe_{2-x}$ under ambient pressure

In order to refine the lattice constants, some single crystals were grinded into powders, and then obtain the X-ray powder diffraction pattern on Bruker D8 Discovery X-ray diffractometer. The powder diffraction pattern is refined by Rietveld method using GSAS-II software, and the Rietveld refinement result is shown here. The overall weighted profile R-factor, Rwp, is 6.97%. Goodness of fit is 1.48. The Rietveld refinement are carried and the lattice parameters are determined with a=3.8553Å, c=5.2630Å, which is smaller than in the previous report a = 3.8776 Å, c = 5.2653 Å [Pressure-driven Lifshitz transition in type-II Dirac semimetal NiTe2, Phys. Rev. B 101, 115124].

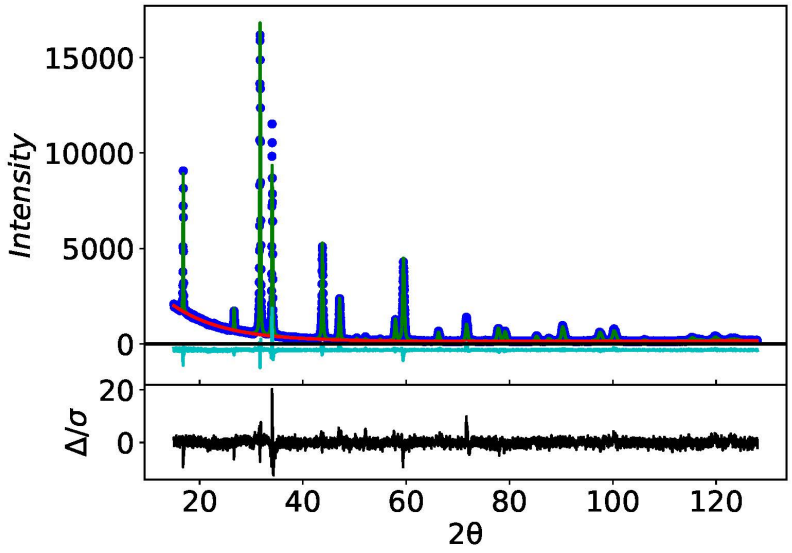

Figure S1. The Rietveld refinement result of the ambient XRD.

2. Electron diffraction spectroscopy (EDS) analyses of the $NiTe_{2-x}$ compositions

The sample compositions were checked by two scanning electron microscopes (SEM): One was SU 5000 (Hitachi, Japan), the other was Gemini SEM 300(Carl Zeiss, Germany). The following figures illustrate the measurement process.

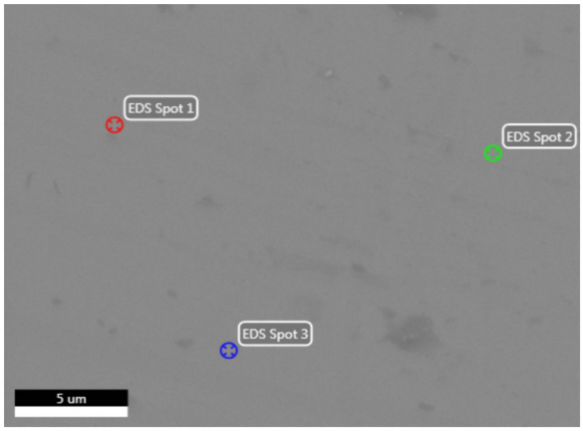

Figure S2. SEM image of the surface of a $NiTe_{2-x}$ single crystal, showing three separate spots where EDS studies were taken by SU 5000 (Hitachi, Japan).

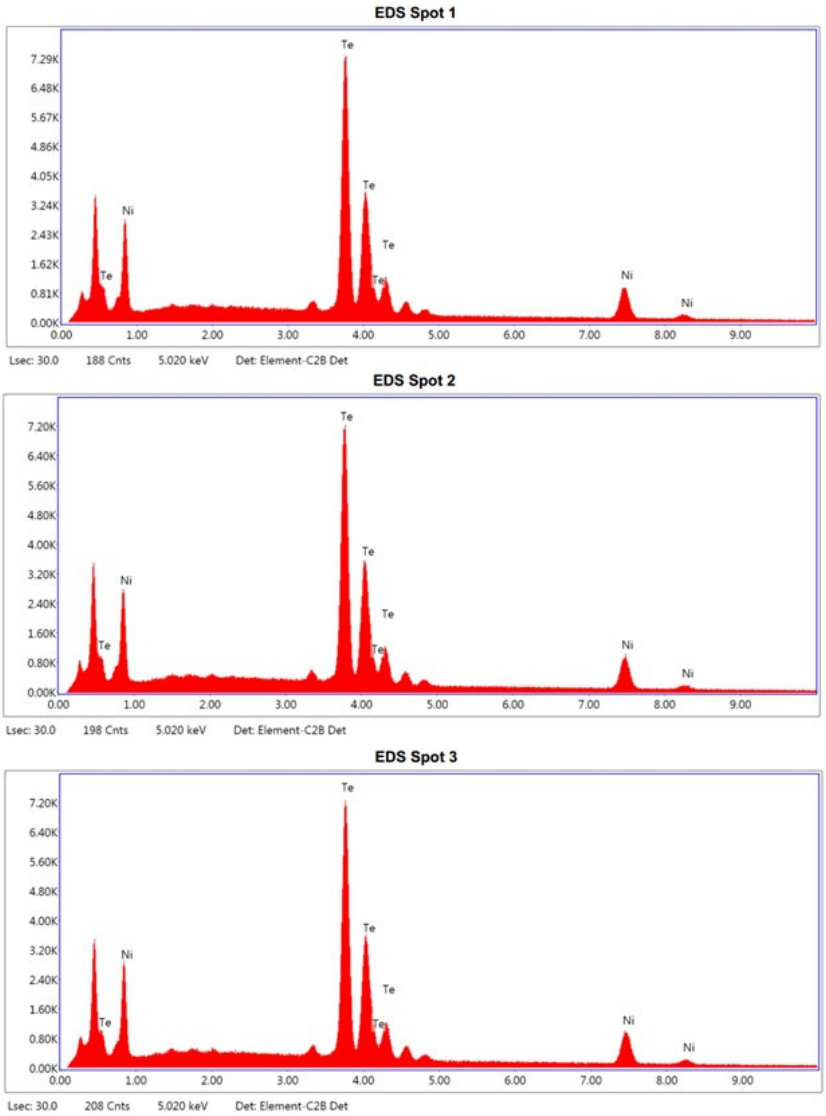

Figure S3. EDS analyses of the sample compositions taken at the three spots shown in Figure S3. The results are summarized in the table below.

Region	Ni (atomic rate/%)	Te(atomic rate/%)
Spot 1	36.61	63.39
Spot 2	36.86	63.14
Spot 3	37.36	62.64
average	**36.94**	**63.06**

Average Ni:Te = 1:1.707 ≈1.71.

a

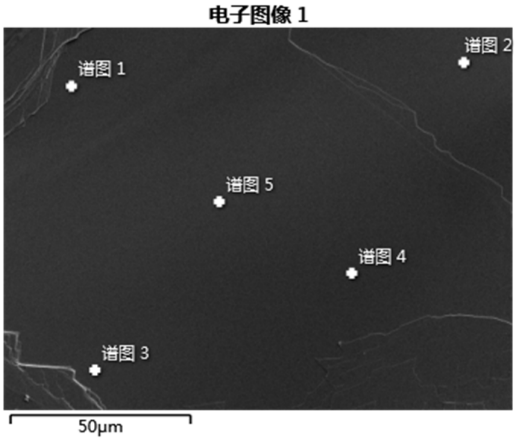

b

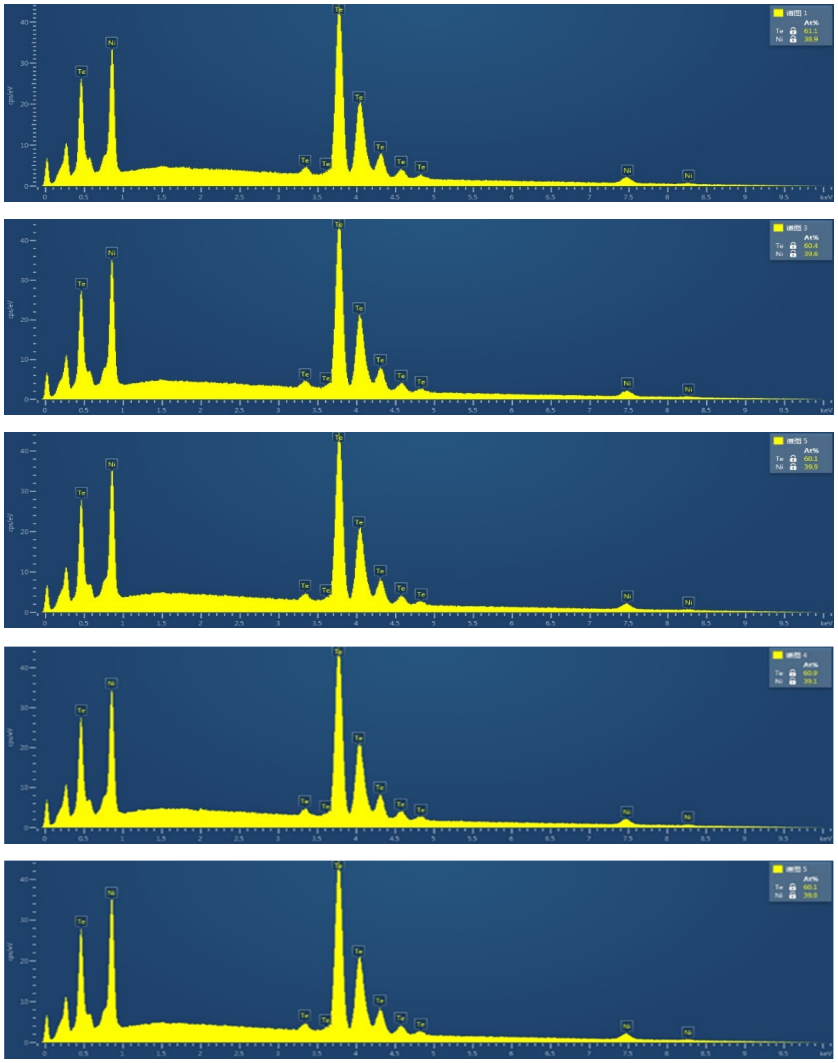

Figure S4. a, SEM image of the surface of a $NiTe_{2-x}$ single crystal, showing five separate spots where EDS studies were taken on Gemini SEM 300 (Carl Zeiss, Germany). **b,** EDS analyses of the sample compositions of the five selected points, and the results are summarized in the table below.

Region	Ni (atomic rate/%)	Te (atomic rate/%)
Spot 1	38.86	61.14
Spot 2	40.07	59.93
Spot 3	39.57	60.43
Spot 4	39.08	60.92
Spot 5	39.91	60.09
average	39.50	60.50

Average Ni: Te = 1: 1.532 (≈ 1.53)

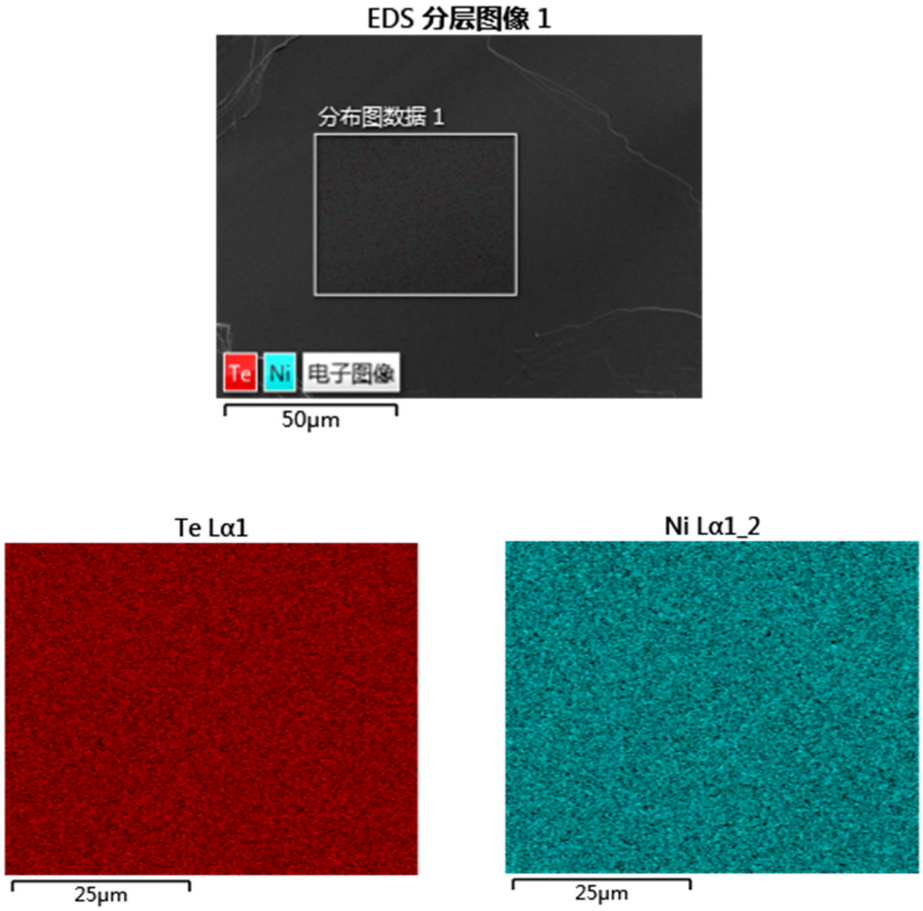

Figure S5. Energy dispersive X-ray spectral mapping of the Te and Ni elements (bottom two panels) in a $NiTe_{2-x}$ single crystal over the squared region indicated on the SEM micrograph (top panel), showing uniform spatial distributions of both Te and Ni elements.

3. Results from the density functional theory (DFT) calculations:

[1] Electronic density of states (DOS) of NiTe (M-phase) under high pressures P = 18 and 42 GPa, and of $NiTe_2$ and $NiTe_{1.625}$ (H-phase) at P = 0 (Figures. S6a-d); [2] Comparison of the DOS of $NiTe_2$ (H-phase) under P = 0, 18 and 42 GPa (Figures. S7a-c); [3] First Brillouin zones of $NiTe_2$ (H-phase, Figure. S8a) and NiTe (M-phase, Figure. S8b); [4] Comparison of the electronic bandstructures of $NiTe_2$ (H-phase, P = 0, Figure. S9a) and NiTe (M-phase, P = 18 GPa, Figure. S9b); [5] Comparison of the electronic bandstructures of $NiTe_2$ (H-phase, P = 18 GPa, Figure. S10a) and $NiTe_2$ (H-phase, P = 42 GPa, Figure. S10b).

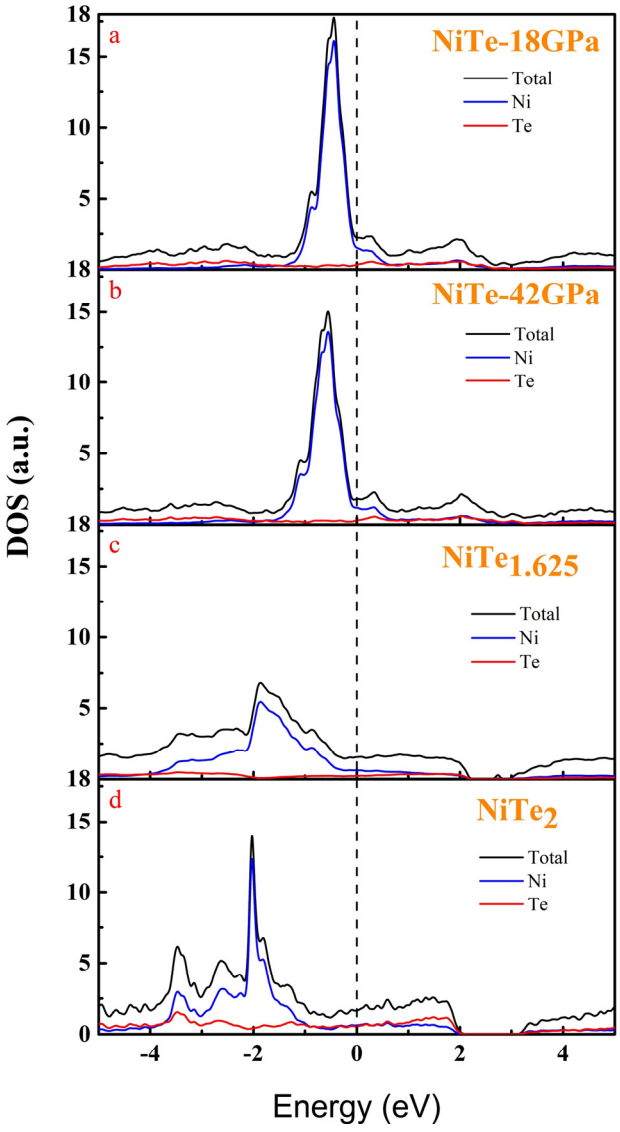

Figure S6. DOS *vs.* energy for NiTe (P = 18 GPa), NiTe (P = 42 GPa), $NiTe_{1.625}$ (P = 0) and $NiTe_2$ (P = 0), respectively. The zero energy point denotes the Fermi level E_F for the respective compound. We note that the DOS associated with the Ni 3*d*-bands is apparently dominant at the Fermi level in the high-pressure phase NiTe (M-phase), whereas both Ni-3*d* and Te-5*p* bands contribute equally at the Fermi level for ambient pressure $NiTe_2$ (H-phase).

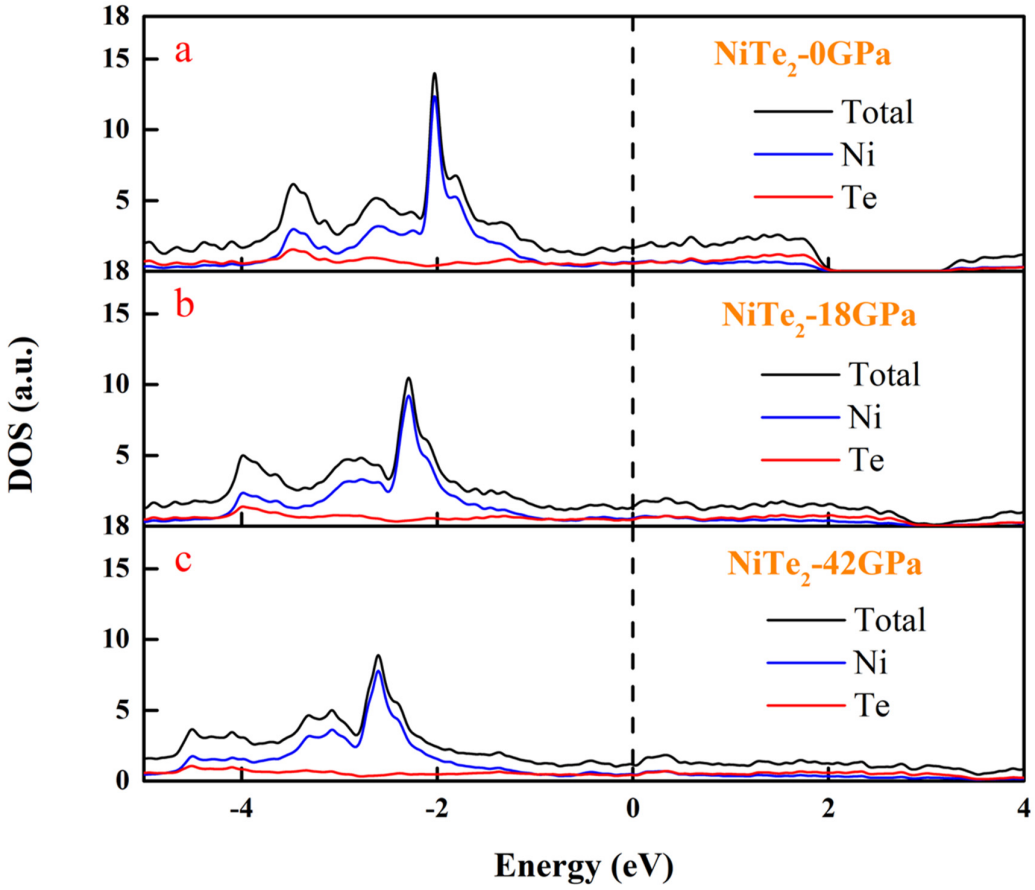

Figure S7. Comparison of the electronic DOS *vs.* energy for $NiTe_2$ (H-phase) at **a,** $P = 0$, **b,** $P = 18$ GPa, and **c,** $P = 42$ GPa. We note that the DOS near the Fermi level E_F steadily decreases with increasing pressure, which is consistent with the empirical findings of decreasing electrical conductivity with increasing pressure found in $NiTe_{1.98}$.[27] Additionally, the Ni-3*d* and Te-5*p* bands at high pressures remain contributing comparably to the DOS near E_F, which differ from the dominant contributions from Ni-3*d* bands in the M-phase under high pressures, as shown in Figures. S6a-b.

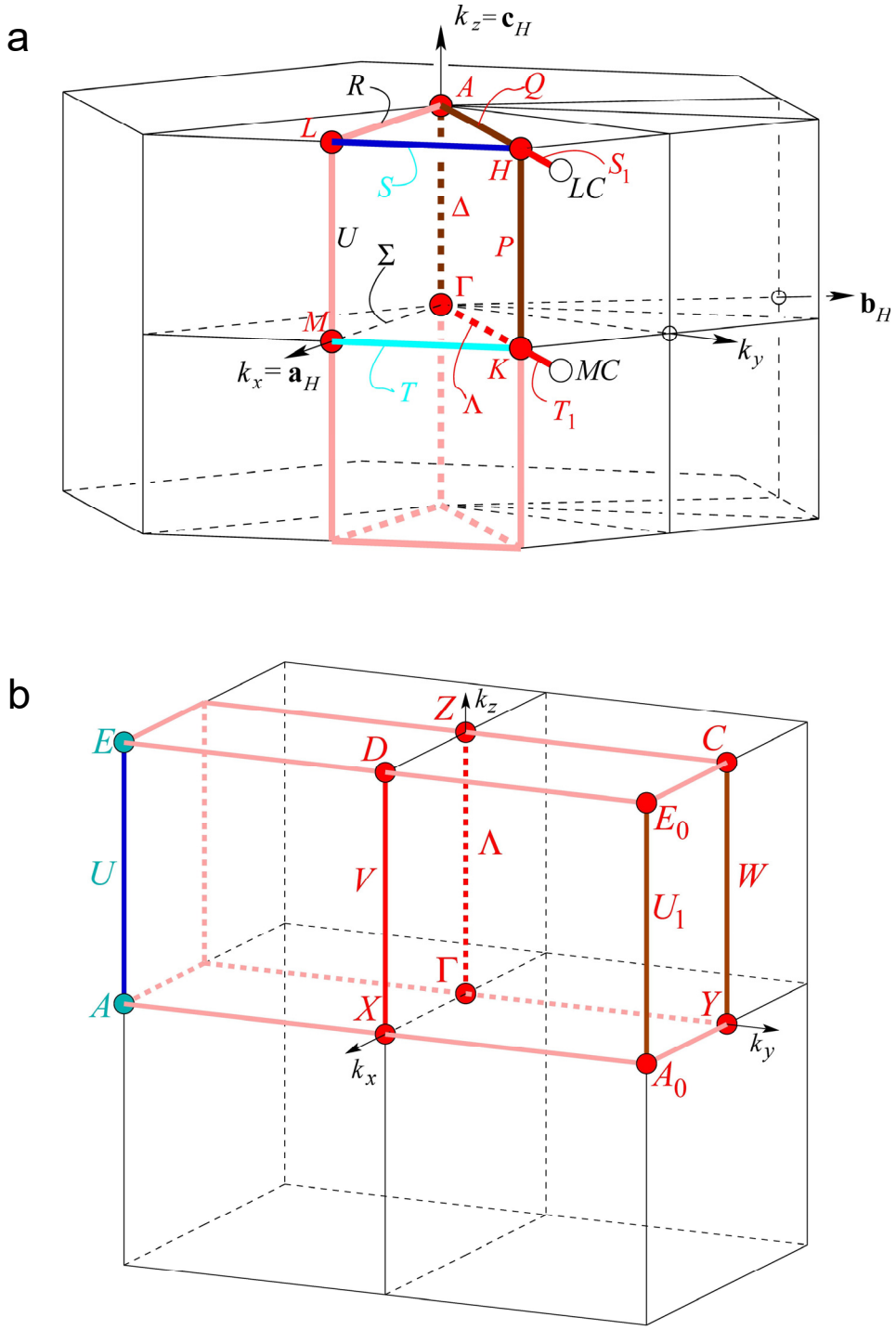

Figure S8. The first Brillouin zone and the high-symmetry points of **a,** $NiTe_2$ (H-phase) with P $\bar{3}$ *m*1 symmetry and **b,** NiTe (M-phae) with P2/m symmetry.

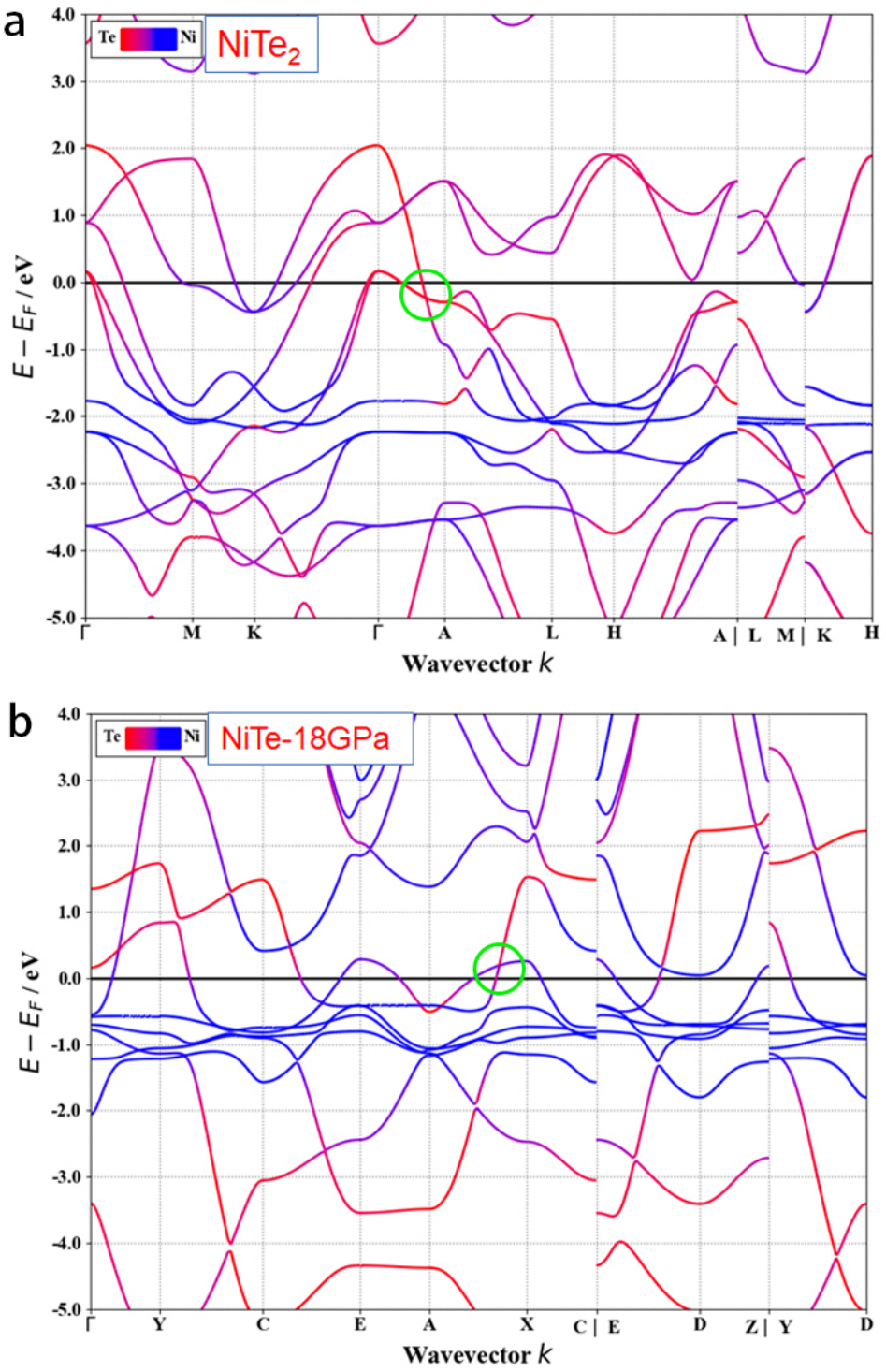

Figure S9. The electronic bandstructures of **a,** $NiTe_2$ (H-phase) at $P = 0$, and **b,** NiTe (M-phase) at $P = 18$ GPa. We note that in $NiTe_2$ the Dirac point closest to the Fermi level ($E = 0$) exists at $E \sim -0.17$ eV along Γ-A (indicated by the green circle), whereas in NiTe the Dirac point closest to the Fermi level moves to $E \sim +0.17$ eV along A-X (indicated by the green circle), although additional Dirac points not too far from the Fermi level also exist along Γ-Y and C-E.

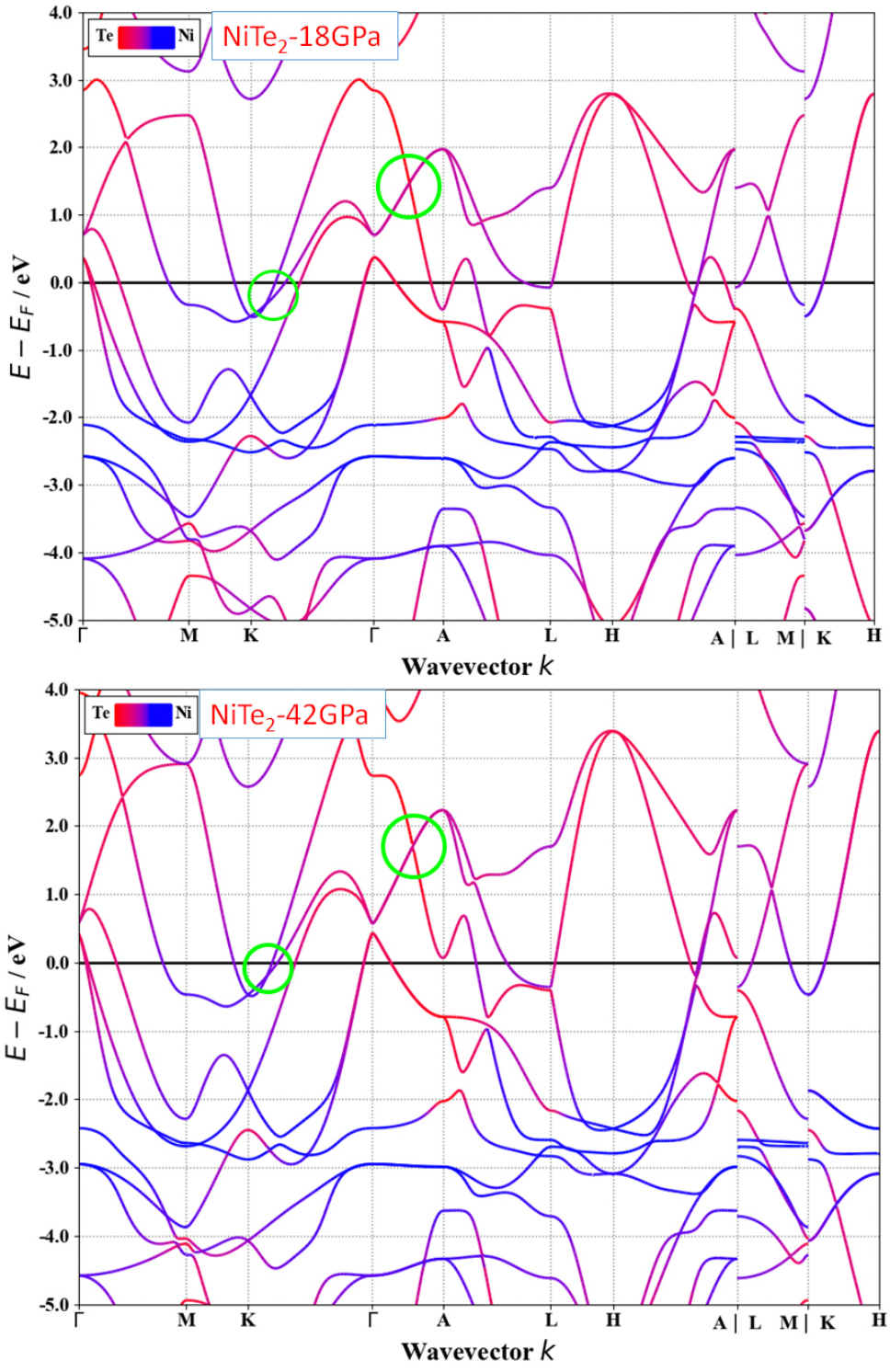

Figure S10. The electronic bandstructures of $NiTe_2$ (H-phase) under high pressures of **a,** P = 18 GPa and **b,** P = 42 GPa. Here we note that the Dirac point found at P = 0 along Γ-A below E_F (Figure. S9a) becomes lifted under high pressure, while new Dirac points appear along K-Γ slightly below E_F and along Γ-A above E_F.